Towards a full-bandwidth numerical acoustic model

Hargreaves, JA and Lam, YW

Proceedings of Meetings on Acoustics

Volume 19, 2013 http://acousticalsociety.org/

ICA 2013 Montreal
Montreal, Canada
2 - 7 June 2013

Architectural Acoustics
Session 4aAAa: Room Acoustics Computer Simulation I

4aAAa1. Towards a full-bandwidth numerical acoustic model

Jonathan A. Hargreaves and Y. Lam*

***Corresponding author's address: Acoustics Research Centre, University of Salford, Salford, M5 4WT, Salford, United Kingdom, y.w.lam@salford.ac.uk**

Prediction models are at the heart of modern acoustic engineering. Current commercial room acoustic simulation software almost exclusively approximates the propagation of sound geometrically as rays or beams. These assumptions yield efficient algorithms, but the maximum accuracy they can achieve is limited by how well the geometric assumption represents sound propagation in a given space. This comprises their accuracy at low frequencies in particular. Methods that directly model wave effects are more accurate but they have a computational cost that scales with problem size and frequency, effectively limiting them to small or low frequency scenarios. This paper will report the results of initial research into a new full-bandwidth model which aims to be accurate and efficient for all frequencies; the name proposed for this is the "Wave Matching Method". This builds on the Boundary Element Method with the premise that if an appropriate interpolation scheme is designed then the model will become 'geometrically dominated' at high frequencies. Other propagation modes may then be removed without significant error, yielding an algorithm which is accurate and efficient. This paper will present the general concepts of wave matching and the results from some numerical test cases.

Published by the Acoustical Society of America through the American Institute of Physics

 [DOI: 10.1121/1.4800226]
Received 22 Jan 2013; published 2 Jun 2013

INTRODUCTION

Prediction models are at the heart of modern acoustic engineering and are used in a diverse range of applications from refining the acoustic design of classrooms and concert halls to predicting how noise exposure varies through an urban environment. Current commercial room acoustic simulation software almost exclusively approximates the propagation of sound geometrically; early reflections are typically evaluated deterministically using a variant of Ray Tracing/Image Source method and late time reverberation is estimated stochastically on the assumption that its distribution matches that of propagated rays. These assumptions yield efficient algorithms, but the maximum accuracy they can achieve is limited by how well the geometric assumption represents sound propagation in a given space. Errors may be significant in certain circumstances, especially at lower frequencies or in smaller rooms.

Methods that model wave effects directly, such as the Boundary Element Method (BEM) and the Finite Element Method (FEM), do not suffer from this shortcoming. BEM has been shown to be an excellent choice for room acoustic simulation, particularly when the priority is to extremely accurately predict scattering from small objects in anechoic conditions[1,2], hence it can greatly accelerate and reduce the cost of prototyping new and innovative acoustic treatments. In addition the mathematical theory behind BEM and FEM is well understood and theoretical error bounds are available such that algorithms can be adapted to guarantee required accuracy; in this sense they are said to have "controllable" error. However they have a computational cost and memory requirement that scales with badly problem size and frequency, effectively limiting them to small or low frequency scenarios. In particular the number of degrees of freedom required by a BEM model grows with frequency and/or geometry size squared and the number of coefficients in the (full) interaction matrices grows with frequency and/or geometry size to the power four. The latter can be thought of as the major bottleneck in the BEM algorithm, both in terms of memory requirements and the computational cost of linear algebra. This is to an extent addressed by the Fast Multipole Method[3], however the number of degrees of freedom required remains unchanged.

In contrast, the success of geometric methods at high-frequencies tells us that good results can be achieved with a much smaller number of degrees of freedom. Hybrid BEMs, where a known geometric solution for a specific geometry is used to design a bespoke discretisation scheme, are achieving excellent progress and can deliver extremely efficient algorithms with controllable error[4]; however these are presently limited to specific scattering object shapes and largely to two-dimensions. In this paper the end objectives are similar, but a more physically-motivated approach will be followed in 3D with the aim of unifying BEM with geometric approaches.

The method described herein is a prototype BEM formulation which we are calling 'Wave Matching'. The fundamental differences between this and a standard BEM are that: 1) surface quantities are discretised using wave-modes instead of elements; 2) a novel testing integral is used. We believe that BEM is a good place to start in a search to unify wave and geometric approaches since both classes of algorithm work with surface geometry and analytically compute how elementary sound sources propagate through the media unobstructed, so the problem is one of computing the reflections and scattering from obstacles. The fundamental difference between BEM and geometric methods is that BEM attacks the problem by numerical discretisation of the total field whereas geometric methods trace reflections individually according to a high-frequency asymptotic approximation. The premise in this paper is that if an appropriate family of oscillatory wave-modes is used as a BEM discretisation scheme, then as the frequency is increased the scattering of each mode becomes increasing ray-like and the number which have significant energy remains relatively small. Accordingly this method should retain low frequency accuracy and controllable error, since it is simply another approach to discretisation, but offer opportunities for acceleration at high frequencies. Numerically this means that although the number of degrees of freedom and the dimensions of the interaction matrices must still grow with problem size and frequency squared, all but a relatively small number of coefficients will be close to zero[5]. This paper extends the research in referece 5 by constructing a full interaction matrix (including self-interaction) for the test case problem of scattering by a 1m^2 cube and examining what trade-off between % matrix population and % error can be achieved by setting small interaction coefficients to zero.

FORMULATION

Figure 1a depicts a scattering problem, comprising an obstacle submerged in a connected domain Ω_+ containing air with equilibrium density ρ_0 and speed of sound c. S is a surface conformal to the obstacle, thus the obstacle resides in the interior domain Ω_-. S_∞ is the extent of the medium; it may be shown that if Sommerfield's radiation condition is satisfied here then there is no reflection and this may be ignored in the integrals that follow. $\mathbf{x}$ and $\mathbf{y}$ are 3D Cartesian vectors defining the observation and radiation points respectively and $R = |\mathbf{x} - \mathbf{y}|$ is the distance

between them. $\mathbf{y}$ is taken to be a point on S and $\hat{\mathbf{n}}_\mathbf{y}$ is the surface-normal unit vector there. $\mathbf{x}$ may lie anywhere in Ω_+ or in Ω_-, including on S; in the case where $\mathbf{x}$ lies on S then $\hat{\mathbf{n}}_\mathbf{x}$ is the surface-normal unit vector there. Total pressure $\varphi(\mathbf{x})$ in the medium is a sum of the incident pressure $\chi(\mathbf{x})$ arriving from sources and the scattered pressure $\psi(\mathbf{x})$ which emanates out from the obstacle in response to this. It is assumed that all acoustic quantities vary periodically in time with angular frequency ω (i.e. $\varphi(\mathbf{x},t) = \varphi(\mathbf{x})e^{-i\omega t}$) and satisfy Helmholtz equation: $\nabla^2\varphi + k^2\varphi = 0$, where $k = \omega/c$ is the wavenumber in radians per meter. Application of Green's theorem in the domain Ω_+ produces the Kirchhoff integral equation (from here on to be called the scattering integral) which allows the scattered sound $\psi(\mathbf{x})$ to be evaluated from the total sound $\varphi(\mathbf{y})$ on S. In the case of a rigid obstacle the latter term is omitted:

$$\psi(\mathbf{x}) = \iint_S \left[\varphi(\mathbf{y})\frac{\partial G}{\partial n_y}(\mathbf{x},\mathbf{y}) - G(\mathbf{x},\mathbf{y})\frac{\partial \varphi}{\partial n_y}(\mathbf{y})\right] d\mathbf{y} \tag{1}$$

Figure 1b depicts the three distinct phases by which a BEM solves the scattering problem. First the incident sound $\chi(\mathbf{y})$ arriving at the obstacle from the sources is calculated using a testing integral. Second the total sound $\varphi(\mathbf{y})$ at the surface of the obstacle is solved for. This includes consideration how the scattered sound from some parts of the obstacle hits other parts of the obstacle and causes further scattering, hence both the testing and scattering integrals are involved and a linear system of equations is produced which must be solved numerically. This stage of the algorithm must also be coupled to some model of the obstacle's acoustic properties (typically locally-reacting surface impedance). Finally the scattered sound $\psi(\mathbf{x})$ at any receivers is calculated from the solution for the total surface sound $\varphi(\mathbf{y})$ using the scattering integral.

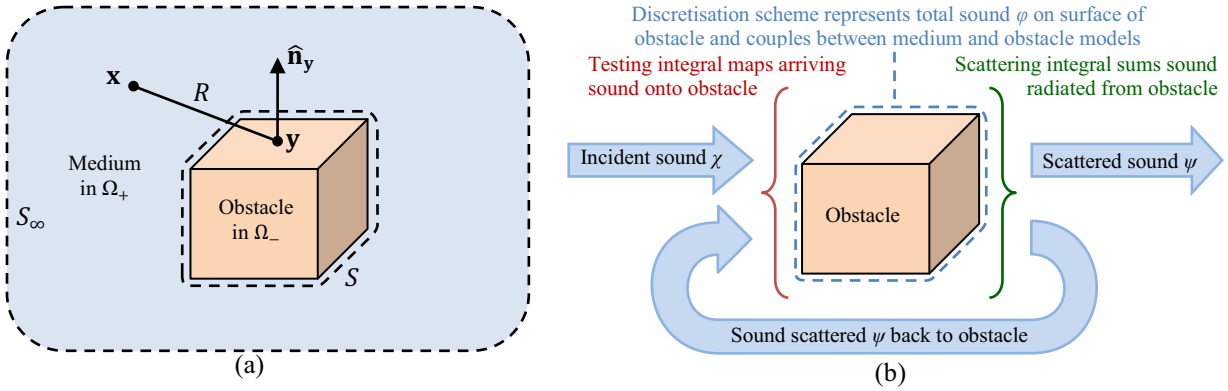

FIGURE 1. a) Geometry of scattering by an obstacle; b) Corresponding BEM solution process

Discretisation of Sound for a Rigid Obstacle with Planar Rectangular Faces

In most BEM formulations the surface is partitioned into a large number of elements, which are all small with respect to wavelength, and on each element a small number of low-order polynomial basis functions are used. There are however other families of functions which could be used to discretised sound at the surface. One option which has attracted attention is the use of oscillatory basis functions[6,7], since these might be able to capture some of the oscillatory behavior of the solution allowing larger elements for the same accuracy. In the Wave Matching approach this idea is taken a step further and the basis functions are chosen to be slices (on S) through waves (i.e. the basis functions themselves satisfy Helmholtz equation). Examples of such waves could include spherical harmonics or families of plane waves; the latter will be used in this test case. The expected benefits of this are three-fold: 1) that both the scattering and testing integrals may be converted from double surface integrals to single contour integrals[5], for evaluation with computational cost which grows only with k instead of k^2; 2) that the need for elements is eliminated and the basis functions may be applied over each smooth obstacle face (so large with respect to wavelength); 3) that a small number of significant coefficients are likely to dominate the interaction matrices and with judicious choice of basis functions it may be possible to represent the solution for accurately $\varphi(\mathbf{y})$ using only a very small number of non-zero weights. It should however be emphasized that these are expected benefits and this paper is a step towards demonstrating that they occur in reality.

Although the test case considered is specified to be a rigid 1m^2 cube, the algorithm will be developed for the slightly broader class of rigid obstacles with planar rectangular faces. Conventional element-based and the new wave-based schemes will be developed in parallel so their performance can be compared.

The surface S bounding the obstacle is comprised of N_f planar rectangular faces. Each face F_a is defined by a corner vector $\mathbf{v}_{a;0}$ and two perpendicular edge vectors $\mathbf{v}_{a;1}$ and $\mathbf{v}_{a;2}$, with normal vector $\hat{\mathbf{n}}_a = \hat{\mathbf{v}}_{a;1} \times \hat{\mathbf{v}}_{a;2}$.

$$S = \bigcup_{a=0}^{N_f-1} F_a \tag{2}$$

In the element-based mode of discretisation, each face F_a is subdivided into a M_a by N_a grid of small rectangular elements $E_{a,m,n}$ with centers at $\mathbf{e}^{\mathrm{c}}_{a,m,n} = \mathbf{v}_{a;0} + [m + 1/2]/M_a\, \mathbf{v}_{a;1} + [n + 1/2]/N_a\, \mathbf{v}_{a;2}$. To achieve eight elements per wavelength we set $M_a = \lceil 4k|\mathbf{v}_{a;1}|/\pi \rceil$ and $N_a = \lceil 4k|\mathbf{v}_{a;2}|/\pi \rceil$, and for the 1m^2 cube under test, $N_f = 6$ and $M_a = N_a = \lceil 4k/\pi \rceil$ for all F_a.

On each element $E_{a,m,n}$ a piecewise-constant basis function $\mathrm{e}_{a,m,n}$ is defined:

$$\mathrm{e}_{a,m,n}(\mathbf{y}) \stackrel{\text{def}}{=} \begin{cases} 1 & \text{if } \mathbf{y} \in E_{a,m,n} \\ 0 & \text{otherwise} \end{cases} \tag{3}$$

The total pressure φ on the surface is approximated by a weighted sum of these; note the superscript "e" on the weights which denotes that they apply to the element-based scheme:

$$\varphi(\mathbf{y}) \approx \sum_{a=0}^{N_f-1} \sum_{m=0}^{M_a-1} \sum_{n=0}^{N_a-1} \mathbf{w}^{\mathrm{e}}_a(m,n)\mathrm{e}_{a,m,n}(\mathbf{y}) \tag{4}$$

The pressure scattered by a single basis function is given as:

$$\psi^{\mathrm{e}}_{a,m,n}(\mathbf{x}) = \iint_S \mathrm{e}_{a,m,n}(\mathbf{y}) \frac{\partial G}{\partial n_y}(\mathbf{x},\mathbf{y}) d\mathbf{y} \tag{5}$$

The wave-basis scheme uses a two-dimensional Fourier series to approximate the pressure on each face. This is particularly suitable for rectangular faces since the basis functions are exactly orthogonal; they are defined:

$$\mathrm{f}_{a,m,n}(\mathbf{y}) \stackrel{\text{def}}{=} \begin{cases} e^{i[\mathbf{y}-\mathbf{e}^{\mathrm{c}}_{a,0,0}]\cdot\mathbf{k}_{a,m,n}} & \text{if } \mathbf{y} \in F_a \\ 0 & \text{otherwise} \end{cases} \tag{6}$$

Here m and n are spatial harmonic indexes and $\mathbf{k}_{a,m,n}$ is defined as:

$$\mathbf{k}_{a,m,n} \stackrel{\text{def}}{=} \frac{2\pi m}{|\mathbf{v}_{a;1}|}\hat{\mathbf{v}}_{a;1} + \frac{2\pi n}{|\mathbf{v}_{a;2}|}\hat{\mathbf{v}}_{a;2} - \hat{\mathbf{n}}_a \sqrt{k^2 - \left(2\pi m/|\mathbf{v}_{a;1}|\right)^2 - \left(2\pi n/|\mathbf{v}_{a;2}|\right)^2} \tag{7}$$

The total pressure φ on the surface is approximated by a weighted sum of these; note the superscript "f" on the weights which denotes that they apply to the Fourier-based scheme:

$$\varphi(\mathbf{y}) \approx \sum_{a=0}^{N_f-1} \sum_{m=-M_a/2}^{M_a/2-1} \sum_{n=-N_a/2}^{N_a/2-1} \mathbf{w}^{\mathrm{f}}_a(m,n)\mathrm{f}_{a,m,n}(\mathbf{y}) \tag{8}$$

It should be noted that each $\mathrm{f}_{a,m,n}(\mathbf{y})$ really represents two waves which are mirror images in the plane of F_a; one incoming and one outgoing with respect to the obstacle. However the rigid boundary condition on the cube means the reflection coefficient between each pair is always unity, hence they have been collapsed into one basis function to simplify the algorithm and half the number of degrees of freedom; a similar approach was successfully used in the time domain for surface-normal plane waves in reference 8. The surface-normal component of particle velocity is equal and opposite for each wave pair, hence it could be argued that the wave propagation vector for the combined basis (as given in Equation 7) should have zero surface-normal component. However the testing integral (see next section) requires the surface-normal component of the incoming wave, and since $[\mathbf{y} - \mathbf{e}^{\mathrm{c}}_{a,0,0}] \cdot \hat{\mathbf{n}}_a$ is always zero, the incoming wave propagation vector may be safely applied to the combined basis. Accordingly the pressure scattered by a single basis function is written with the surface-normal velocity omitted, since that is zero for the combined basis function pair:

$$\psi^{\mathrm{f}}_{a,m,n}(\mathbf{x}) = \iint_S \mathrm{f}_{a,m,n}(\mathbf{y}) \frac{\partial G}{\partial n_y}(\mathbf{x},\mathbf{y}) d\mathbf{y} \tag{9}$$

Testing Integral

Figure 2 illustrates the conceptual separation between the boundary integral model of the medium and the model of the obstacle's acoustic properties. In many acoustic application the presence of two coupled models is not obvious, since either (as in this test case) the obstacle is considered sound hard and impenetrable, in which case there is no acoustic obstacle model, or it is considered to be locally reacting, in which case a surface impedance model is used and this can be substituted directly into the BEM equations giving the illusion of there being only one model. If the obstacle is sound penetrable and non-locally reacting then the presence of two models becomes clearer, since some sort of FEM (or BEM if the obstacle is has homogeneous acoustic properties) is required for the interior domain Ω_-; these are coupled to the medium model in Ω_+ through the discretisation scheme on S.

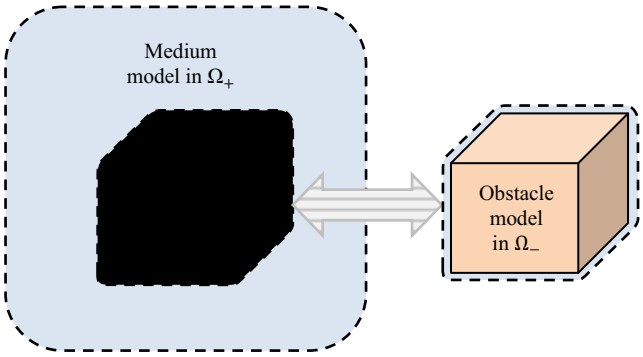

FIGURE 2. Conceptual separation of medium and obstacle models

This is discussed here because it gives insight into what the medium model must achieve in Ω_-, effectively an acoustic black hole in place of the obstacle, from which nothing is reflected (unless passed back from the obstacle model) and through which nothing can pass (unless the obstacle model implements this). The objectives of the testing integral are thus twofold: 1) to provide input data for the model of the obstacle's acoustic properties; 2) to permit scattering of a "shadow" wave into the interior of the obstacle to cancel the incoming sound such that the total acoustic energy (incident plus scattered) within the volume occupied by the obstacle is zero and so that waves cannot pass through the obstacle (unless the obstacle model implements this).

Typically this has been achieved by stipulating that total pressure $\varphi(\mathbf{x}) = 0$ if $\mathbf{x} \in \Omega_-$. However (with the exception of the CHIEF[9] method) it is only possible to enforce this infinitesimally inside S, so instead of being a region of zero pressure Ω_- becomes a soft cavity, which has its own resonances leading to the well documented non-uniqueness problem. It is also well known that using a combination of the pressure and its surface-normal derivative circumvents this problem. In the frequency domain acoustics this is known as the Burton-Miller method[10] but in electromagnetic and time-domain acoustics it is known as the Combined Field Integral Equation (CFIE)[11]; we will use the latter formulation since the normalization factors better suit our application.

The CFIE may be stated in the frequency domain as $ik(1-\alpha)\varphi(\mathbf{x}) = \alpha\, \partial\varphi/\partial n_x\,(\mathbf{x})$, where $0 < \alpha < 1$ is a frequency-independent blend coefficient. Taking the median value $\alpha = {}^1/_2$, we have the condition:

$$ik\varphi(\mathbf{x}) = \frac{\partial \varphi}{\partial n_x}(\mathbf{x}) \tag{10}$$

It is easy to show that Equation 10 is satisfied by any plane wave travelling in the direction $\hat{\mathbf{n}}_\mathbf{x}$, that is, out of the obstacle. The CFIE therefore permits sound emanating from the obstacle model to return to the medium, but discretises sound arriving from the medium, passing that data to the obstacle model and scattering cancelling waves into Ω_-. As a side effect of this, it also permits any small amounts of energy entering Ω_- due to only approximate cancellation of incident and scattered waves to exit into Ω_+ without reflection, hence internal cavity resonances do not occur[12].

It would be desirable to create a variant of the CFIE which is valid for a more general class of waves; in this paper we are specifically interested in plane waves travelling in the direction $\mathbf{k}_{a,m,n}$. To this end we define the testing statement, which matches Equation 10 when $m = n = 0$ and $\mathbf{k}_{a,0,0} = -k\hat{\mathbf{n}}_\mathbf{x}$:

$$\frac{\partial \varphi}{\partial n_x}(\mathbf{x}) + i\hat{\mathbf{n}}_\mathbf{x} \cdot \mathbf{k}_{a,m,n}\varphi(\mathbf{x}) = 0 \tag{11}$$

Because the plane wave basis functions spatially overlap with one another, and because there do not exist locations where all but one are zero, collocation testing is not appropriate and Galerkin testing integrals must be evaluated to achieve a well-conditioned numerical system. The most appropriate testing functions are the complex conjugates of the basis functions, since these de-modulate the oscillation of the form $e^{i\mathbf{y}\cdot\mathbf{k}_{a,m,n}}$. The testing face will be called F_b (i.e. indexed by b) and on it the basis functions will be indexed by p and q, with summation limits P_b and Q_b. Using $\overline{\partial f_{b,p,q}/\partial n_x\,(\mathbf{x})} = -i\hat{\mathbf{n}}_\mathbf{x}\cdot\mathbf{k}_{b,p,q}\overline{f_{b,p,q}(\mathbf{x})}$ we have:

$$\iint_{F_b} \overline{f_{b,p,q}(\mathbf{x})}\left[\frac{\partial\varphi}{\partial n_x}(\mathbf{x}) + i\hat{\mathbf{n}}_\mathbf{x}\cdot\mathbf{k}_{b,p,q}\varphi(\mathbf{x})\right]d\mathbf{x} = \iint_{F_b}\left[\overline{f_{b,p,q}(\mathbf{x})}\frac{\partial\varphi}{\partial n_x}(\mathbf{x}) - \varphi(\mathbf{x})\overline{\frac{\partial f_{b,p,q}}{\partial n_x}}(\mathbf{x})\right]d\mathbf{x} \tag{12}$$

The right hand statement in Equation 12 is very interesting for two reasons. First it bears a very close resemblance to the energy-inspired time domain BEM algorithms in references 13 and 14, for which unconditional stability can be proven. Secondly it bears a close resemblance to the scattering integral, suggesting that transformation to an edge integral for efficient evaluation may be possible; this has yet to be shown but Asvestas[15] gives a process for converting double integrals of this form into contour integrals. Substituting $\varphi(\mathbf{x}) = \psi(\mathbf{x}) + \chi(\mathbf{x})$ and then breaking down $\psi(\mathbf{x})$ into a sum of waves $\psi^{\mathrm{f}}_{a,m,n}(\mathbf{x})$ scattered by each basis function yields:

$$\mathbf{A}^{\mathrm{f}}_{b,a}(p,q,m,n) \stackrel{\text{def}}{=} \iint_{F_b}\overline{f_{b,p,q}(\mathbf{x})}\left[\frac{\partial\psi^{\mathrm{f}}_{a,m,n}}{\partial n_x}(\mathbf{x}) + i\hat{\mathbf{n}}_\mathbf{x}\cdot\mathbf{k}_{b,p,q}\psi^{\mathrm{f}}_{a,m,n}(\mathbf{x})\right]d\mathbf{x} \tag{13}$$

$$\mathbf{b}^{\mathrm{f}}_{b}(p,q) \stackrel{\text{def}}{=} -\iint_{F_b}\overline{f_{b,p,q}(\mathbf{x})}\left[\frac{\partial\chi}{\partial n_x}(\mathbf{x}) + i\hat{\mathbf{n}}_\mathbf{x}\cdot\mathbf{k}_{b,p,q}\chi(\mathbf{x})\right]d\mathbf{x} \tag{14}$$

Because each face uses two discretisation indexes the interaction matrices are four-dimensional, though it is straightforward to reshape them to two-dimensions for use with standard matrix solver. The reshaped matrices are concatenated as follows to give a matrix equation $\mathbf{Aw} = \mathbf{b}$ which may be solved numerically to find the vector of discretisation weights $\mathbf{w}$:

$$\mathbf{A} = \begin{bmatrix}\mathbf{A}_{0,0} & \cdots & \mathbf{A}_{0,N_f-1}\\ \vdots & \ddots & \vdots \\ \mathbf{A}_{N_f-1,0} & \cdots & \mathbf{A}_{N_f-1,N_f-1}\end{bmatrix} \qquad \mathbf{b} = \begin{bmatrix}\mathbf{b}_0\\ \vdots \\ \mathbf{b}_{N_f-1}\end{bmatrix} \qquad \mathbf{w} = \begin{bmatrix}\mathbf{w}_0\\ \vdots \\ \mathbf{w}_{N_f-1}\end{bmatrix} \tag{15}$$

Numerical Implementation

The element based scheme is tested in a similar manner to above. Some intermediary quantities are defined:

$$\begin{aligned}\mathbf{K}^{\mathrm{e}}_{b,a}(p,q,m,n) &\stackrel{\text{def}}{=} \iint_S \mathrm{e}_{b,p,q}(\mathbf{x})\iint_S \mathrm{e}_{a,m,n}(\mathbf{y})\frac{\partial G}{\partial n_y}(\mathbf{x},\mathbf{y})d\mathbf{y}\,d\mathbf{x}\\ &= \iint_{\mathrm{E}_{b,p,q}}\iint_{\mathrm{E}_{a,m,n}}\frac{\partial G}{\partial n_y}(\mathbf{x},\mathbf{y})d\mathbf{y}\,d\mathbf{x}\end{aligned} \tag{16}$$

$$\begin{aligned}\mathbf{D}^{\mathrm{e}}_{b,a}(p,q,m,n) &\stackrel{\text{def}}{=} \iint_S \mathrm{e}_{b,p,q}(\mathbf{x})\iint_S \mathrm{e}_{a,m,n}(\mathbf{y})\frac{\partial^2 G}{\partial n_y\partial n_x}(\mathbf{x},\mathbf{y})d\mathbf{y}\,d\mathbf{x}\\ &= \iint_{\mathrm{E}_{b,p,q}}\iint_{\mathrm{E}_{a,m,n}}\frac{\partial^2 G}{\partial n_y\partial n_x}(\mathbf{x},\mathbf{y})d\mathbf{y}\,d\mathbf{x}\end{aligned} \tag{17}$$

These integrals above are evaluated using standard numerical techniques, with just single-point Quadrature on the outer integral but proper care being taken to regularise the singularities in the inner-kernel. The element-based interaction matrices use the CFIE hence:

$$\mathbf{A}^{\mathrm{e}}_{b,a} = \mathbf{D}^{\mathrm{e}}_{b,a} - ik\mathbf{K}^{\mathrm{e}}_{b,a} \tag{18}$$

The excitation wave is a plane wave with propagation direction $\hat{\mathbf{k}}_\chi$, so $\chi(\mathbf{x}) = e^{i\mathbf{k}_\chi\cdot\mathbf{x}}$ and $\partial\chi/\partial n_x = i\hat{\mathbf{n}}_b\cdot\mathbf{k}_\chi\chi$:

$$\mathbf{b}^{\mathrm{e}}_{b}(p,q) = -i\left[\hat{\mathbf{n}}_b\cdot\mathbf{k}_\chi - k\right]\iint_{E_{b,p,q}}\chi(\mathbf{x})\,d\mathbf{x} \tag{19}$$

For the wave-based scheme the intermediate matrices are defined as:

$$\mathbf{K}^{\mathrm{f}}_{b,a}(p,q,m,n) \stackrel{\text{def}}{\equiv} \iint_S \overline{f_{b,p,q}(\mathbf{x})} \iint_S f_{a,m,n}(\mathbf{y}) \frac{\partial G}{\partial n_y}(\mathbf{x},\mathbf{y}) d\mathbf{y}\, d\mathbf{x} \tag{20}$$

$$\mathbf{D}^{\mathrm{f}}_{b,a}(p,q,m,n) \stackrel{\text{def}}{\equiv} \iint_S \overline{f_{b,p,q}(\mathbf{x})} \iint_S f_{a,m,n}(\mathbf{y}) \frac{\partial^2 G}{\partial n_y \partial n_x}(\mathbf{x},\mathbf{y}) d\mathbf{y}\, d\mathbf{x} \tag{21}$$

These combine to give the wave-matching testing integral:

$$\mathbf{A}^{\mathrm{f}}_{b,a}(p,q,m,n) = \mathbf{D}^{\mathrm{f}}_{b,a}(p,q,m,n) + i\hat{\mathbf{n}}_a \cdot \mathbf{k}_{a,m,n} \mathbf{K}^{\mathrm{f}}_{b,a}(p,q,m,n) \tag{22}$$

The excitation vectors is given by:

$$\mathbf{b}^{\mathrm{f}}_b(p,q) = -i\left[\hat{\mathbf{n}}_b \cdot \mathbf{k}_\chi + \hat{\mathbf{n}}_b \cdot \mathbf{k}_{b,p,q}\right] \iint_{F_b} \overline{\mathrm{f}_{b,p,q}(\mathbf{x})}\, \chi(\mathbf{x})\, d\mathbf{x} \tag{23}$$

Equations 20 and 21 are less well studied than Equations 16 and 17 and direct numerical integration schemes are still under development. However it is possible to numerically evaluated Equation 20 from Equation 16 and Equation 21 from Equation 17 as follows; this will be demonstrated for the outer integral containing the testing function, but a similar process applies to the inner integral too.

With a little manipulation it can be shown that the testing function at the element centres has the same form as a two-dimensional discrete Fourier transform (DFT):

$$\overline{f_{b,p,q}\left(\mathbf{e}^{\mathrm{c}}_{b,p',q'}\right)} = e^{-i\frac{2\pi}{P_b}pp'} e^{-i\frac{2\pi}{Q_b}qq'} \tag{24}$$

If the wave basis is approximated by elements then a DFT type statement arise:

$$\begin{aligned} \overline{f_{b,p,q}(\mathbf{x})} &\approx \sum_{p'=0}^{P_b-1} \sum_{q'=0}^{Q_b-1} \overline{f_{b,p,q}\left(\mathbf{e}^{\mathrm{c}}_{b,p',q'}\right)} \mathrm{e}_{b,p',q'}(\mathbf{x}) \\ &= \sum_{p'=0}^{P_b-1} \sum_{q'=0}^{Q_b-1} e^{-i\frac{2\pi}{P_b}pp'} e^{-i\frac{2\pi}{Q_b}qq'} \mathrm{e}_{b,p',q'}(\mathbf{x}) \end{aligned} \tag{25}$$

Substituting this (and a similar statement over the scattering face) into Equation 20 and Equation 21 allows $\mathbf{K}$ and $\mathbf{D}$ to be calculated by a 4D $\mathcal{FFT}$, where $\boldsymbol{m}(p,q,m,n) = m$, and $\boldsymbol{n}(p,q,m,n) = n$, and $\mathbf{b}$ by a 2D $\mathcal{FFT}$:

$$\mathbf{K}^{\mathrm{f}}_{b,a} = e^{-2i\pi\left[\frac{\boldsymbol{m}}{M_a}+\frac{\boldsymbol{n}}{N_a}\right]} \mathcal{FFT}^4 \left\{ \underset{3,4}{\mathrm{flip}}\left(\mathbf{K}^{\mathrm{e}}_{b,a}\right) \right\} \tag{26}$$

$$\mathbf{D}^{\mathrm{f}}_{b,a} = e^{-2i\pi\left[\frac{\boldsymbol{m}}{M_a}+\frac{\boldsymbol{n}}{N_a}\right]} \mathcal{FFT}^4 \left\{ \underset{3,4}{\mathrm{flip}}\left(\mathbf{D}^{\mathrm{e}}_{b,a}\right) \right\} \tag{27}$$

$$\mathbf{b}^{\mathrm{f}}_b = \mathcal{FFT}^2\{\mathbf{b}^{\mathrm{e}}_b\} \tag{28}$$

Since $f_{a,m,n}$ has no conjugate extra operations are required to make it fit the form of a DFT: multiplication by $e^{-2i\pi[\boldsymbol{m}/M_a+\boldsymbol{n}/N_a]}$ which implements a spatial shift by one element; application of flip flips the matrix in each of the dimensions listed underneath, hence $\underset{3,4}{\mathrm{flip}}$ is equivalent to `flipdim(flipdim(A,3),4)` in Matlab™.

TEST PROCEDURE AND RESULTS

As discussed earlier, the hypothesis of this paper is that the wave-mode scheme produces interaction matrices which are dominated by a relatively small number of significant terms, and that the remainder may be set to zero without incurring substantial error. This will be tested by progressively culling (i.e. setting to zero) interaction coefficients, starting with the smallest magnitude and gradually moving to the largest, and examining the error that results. Because BEM solutions rely on cancellation and interference between different terms, it is unwise to use a hard cutoff to cull interactions and instead a soft cutoff was devised. This operated by applying a linear taper between two thresholds t_{upper} and t_{lower}, and was stated in such a way that the phase of the complex-valued interaction matrices was retained (see Equation 29 overleaf). In all cases it was chosen that $t_{lower} = 0.1 \times t_{upper}$. An example culling-profile with $t_{upper} = 10^{-3}$ is shown in Figure 3.

$$A_{culled} = \begin{cases} A & |A| > t_{upper} \\ A \times \dfrac{t_{upper}}{|A|} \dfrac{|A| - t_{lower}}{t_{upper} - t_{lower}} & t_{lower} < |A| < t_{upper} \\ 0 & |A| < t_{lowe\,r} \end{cases} \tag{29}$$

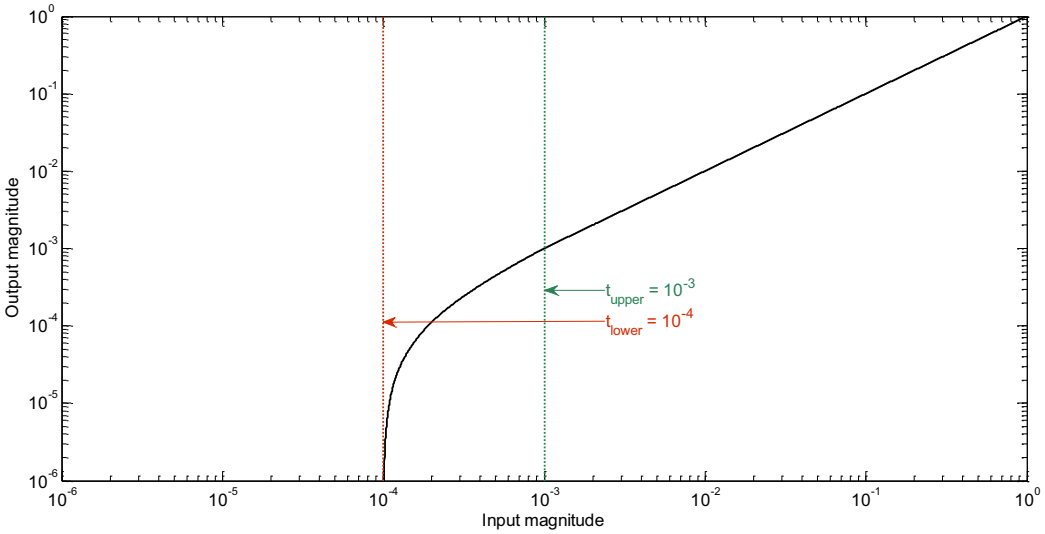

Figure 3. Example Culling Profile with $t_{upper} = 10^{-3}$ and $t_{lower} = 10^{-4}$

Culling was applied to both the A and b matrices, with t_{upper} respectively set as a fraction of the largest magnitude coefficient in each. Solution error incurred through culling was quantified by computing the mean error in the surface pressure at the element centers, normalized by the mean magnitude of the un-culled solution. For the element scheme this could be computed directly from the surface weights (as Equation 30), but for the wave-mode scheme computation of the surface pressures by inverse FFT of the discretisation weights was required beforehand.

$$\text{Normalised Mean Error} = \frac{\text{mean}[\mathbf{w} - \mathbf{w}_{\text{culled}}]}{\text{mean}[\mathbf{w}]} \tag{30}$$

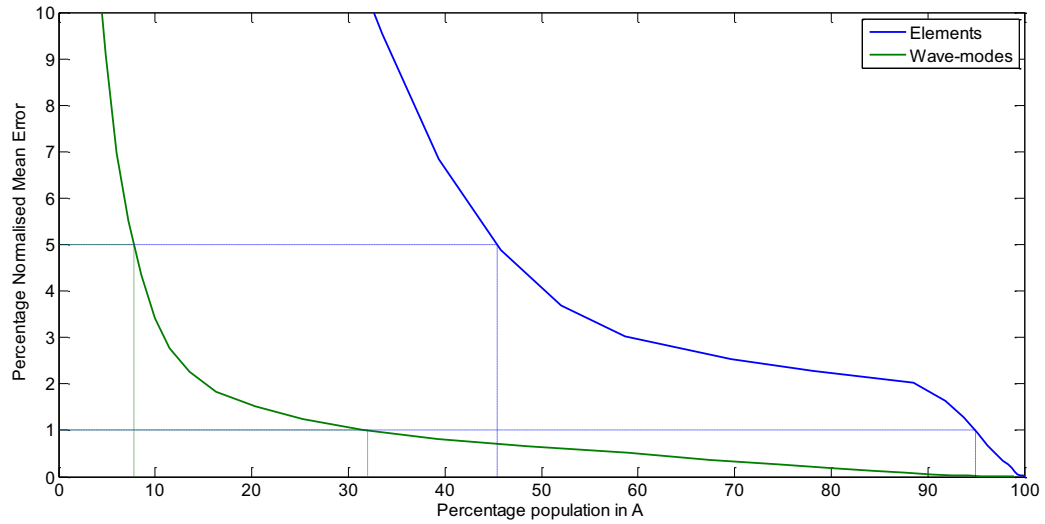

Figure 4. Percentage population of the A matrices vs percentage normalized mean error in the surface pressure for k = 4π. Percentage population required to achieve 1% and 5% error is indicated for each scheme.

Figure 4 shows the trend between percentage population of the A matrices, being the number of non-zeros versus the total number of elements ($N_f \times \lceil 4k/\pi \rceil^4$), and the percentage normalized mean error, as defined in Equation 30. In this test case the wavenumber $k = 4\pi$ and $\mathbf{k}_\chi = [0 \quad 0 \quad -k]$. It is clearly seen that the culling process causes less error in the wave-matching scheme than it does when using conventional elements. To achieve error below 5% the wave-matching scheme requires only 8% of its coefficients to be retained, whereas the element scheme requires 45% to be retained. To achieve error below 1% the wave-matching scheme requires only 32% of its coefficients to be retained, whereas the element scheme requires 95% to be retained.

This is encouraging initial evidence that supports the notion that the use of a wave-matching scheme does indeed allow the interaction matrices to be sparsified. Ongoing research will look at other test cases and examine how the number of interactions which must be retained varies with frequency, since this will inform us as to whether the scheme becomes quasi-geometric at high frequencies as hoped, or just gives a fixed efficiency scaling as other existing oscillatory basis functions have achieved[6,7].

CONCLUSIONS

This paper compared a conventional element-based BEM formulation and a new 'wave-matching' formulation on the problem of scattering by a cube. Small coefficients in the interaction matrices were culled (set to zero) and the error examined. It was found that the wave-matching scheme is more tolerant of culling than the standard elements-based approach, which may provide a means of achieving improved efficiency at high frequencies.

ACKNOWLEDGMENTS

This work was supported by EPSRC grant reference: EP/J022071/1.

REFERENCES

1 T. J. Cox and Y. W. Lam, "Prediction and Evaluation of the Scattering from Quadratic Residue Diffusers", J. Acoust. Soc. Am. **95,** 297–305 (1994)
2 T. J. Cox, "Predicting the scattering from reflectors and diffusers using 2D BEM", J. Acoust. Soc. Am. **96,** 874–878 (1994)
3 S. Amini and A. T. J. Profit, "Multi-level fast multipole solution of the scattering problem", Eng. Anal. Bound. Elem. **27,** 547–564 (2003)
4 S. N. Chandler-Wilde, I. G. Graham, S. Langdon and E. A. Spence, "Numerical-asymptotic boundary integral methods in high frequency acoustic scattering", Acta Numerica **21**, 89-305 (2012)
5 Y. W. Lam and J. A. Hargreaves, "Time Domain Modelling of Room Acoustics. Proceedings of Acoustics 2012", April 2012, Nantes, France
6 E. Perrey-Debain, J. Trevelyan and P. Bettess, "Wave boundary elements: a theoretical overview presenting applications in scattering of short waves", Eng. Anal. Bound. Elem. **28,** 131–141 (2004)
7 H. Beriot, E. Perrey-Debain, M. BenTahar and C. Vayssade, "Plane wave basis in Galerkin BEM for bidimensional wave scattering" Eng. Anal. Bound. Elem. **34**, 130–143 (2010)
8 J. A. Hargreaves and T. J. Cox, "A transient boundary element method model of Schroeder diffuser scattering using well mouth impedance", J. Acoust. Soc. Am. **124**, 2942–2951 (2008)
9 H. A. Schenck, "Improved integral formulation for acoustic radiation problems", J. Acoust. Soc. Am. **44**, 41–58 (1968)
10 A. J. Burton and G. F. Miller, "The application of integral equation methods to the numerical solution of some exterior boundary-value problems", Proc. R. Soc. London, Ser. A **323**, 201–210 (1971)
11 A. A. Ergin, B. Shanker, and E. Michielssen, "Analysis of transient wave scattering from rigid bodies using a Burton–Miller approach", J. Acoust. Soc. Am. **106**, 2396–2404 (1999).
12 D. J. Chappell, P. J. Harris, D. Henwood and R. Chakrabarti, "A stable boundary integral equation method for modelling transient acoustic radiation", J. Acoust.Soc. Am. **120**, 74–80 (2006)
13 T. Ha-Duong, B. Ludwig and I. Terrasse, " A Galerkin BEM for transient acoustic scattering by an absorbing obstacle", Int. J. Numer. Meth. Engng. **57**, 1845–1882 (2003)
14 A. Aimi, M. Diligenti, C. Guardasoni, I. Mazzieri and S. Panizzi, "An energy approach to space–time Galerkin BEM for wave propagation problems", Int. J. Numer. Meth. Eng. **80**, 1196–1240 (2009)
15 J. S. Asvestas, "Line integrals and physical optics. Part II. The conversion of the Kirchhoff surface integral to a line integral", J. Opt. Soc. Am. A: **2**, 896 - 902 (1985)